Experimental method for *in situ* determination of material textures at simultaneous high pressure and high temperature by means of radial diffraction in the diamond anvil cell

Hanns-Peter Liermann,[1,2] Sébastien Merkel,[3] Lowell Miyagi,[4] Hans-Rudolf Wenk,[4] Guoyin Shen,[1] Hyunchae Cynn,[5] and William J. Evans[5]
[1]*High-Pressure Collaboration Access Team, Geophysical Laboratory, Carnegie Institution of Washington, Argonne, Illinois 60439, USA*
[2]*DESY, Hamburg 22607, Germany*
[3]*Laboratoire de Structure et Propriétés de l'Etat Solide, Université Lille1, CNRS, 59655 Villeneuve d'Ascq Cedex, France*
[4]*Department of Earth and Planetary Science, University of California-Berkeley, California 94720, USA*
[5]*High Pressure Physics Group, Lawrence Livermore National Laboratory, 7000 East Avenue, L-041 Livermore, California 94550, USA*

(Received 23 June 2009; accepted 1 September 2009; published online 13 October 2009)

We introduce the design and capabilities of a resistive heated diamond anvil cell that can be used for side diffraction at simultaneous high pressure and high temperature. The device can be used to study lattice-preferred orientations in polycrystalline samples up to temperatures of 1100 K and pressures of 36 GPa. Capabilities of the instrument are demonstrated with preliminary results on the development of textures in the bcc, fcc, and hcp polymorphs of iron during a nonhydrostatic compression experiment at simultaneous high pressure and high temperature. © *2009 American Institute of Physics.* [doi:10.1063/1.3236365]

I. INTRODUCTION

For many years, diamond anvil cells (DACs) have been used to determine the compression behavior of materials at high pressure.[1] Of particular interest has been the use of the DAC to determine the stress and strain state of minerals and compounds under nonhydrostatic conditions and ambient temperatures using the radial diffraction geometry[2–6] (Fig. 1). Most of these experiments are only possible because of the use of x-ray transparent gaskets, consisting of amorphous B inserts[6–9] or Be[3,4] that allow the collection of x-ray diffraction data from samples perpendicular to the loading axis. Radial diffraction has also been used to study texture and crystallographic preferred orientations (CPOs) in plastically deformed materials[10] by measuring intensity variations along the Debye rings. For instance, texture information was recently used to model the activation of slip systems at high pressure in geological relevant materials such as polycrystalline $(Mg_{0.9},Fe_{0.1})SiO_3$ postperovskite[11] and its Ge analog.[12] However, extrapolation of these findings to high pressure and high temperature conditions of the Earth's lower mantle has proven to be incomplete because of our lack of understanding the effect of temperature on high-pressure plasticity.

There are multiple avenues one might take to study plastic deformation under simultaneous high pressure, high temperature while probing the sample using *in situ* x-ray diffraction: (a) in a large volume press (LVP) such a Drickamer[13] or the multianvil device,[14] (b) in a DAC that is heated internally with a laser,[15] and (c) in a DAC that is heated externally through a resistive heater such as graphite. Each of these techniques has its advantages and disadvantages. While there has been significant progress using different types of LVP to measure stress and textures at simultaneous high pressures and high temperatures, it is currently not possible to use those instruments to perform quantitative deformation experiments beyond pressures of the transition zone (21 GPa and 2000 K). Recently, radial diffraction experiments in the DAC using *in situ* laser heating have made significant progress.[15,16] They are, however, complicated by the presence of large temperature gradients that develop during heating. So far externally heated DACs have not been used for stress and texture analyses because the resistive heater would lie in the x-ray path. A design of a cell capable of such experiments was published recently[17] but has not been tested for radial diffraction experiments. Furthermore, gasket materials typically used in radial diffraction experiments lose their strength at high temperatures (as do diamond anvils) and thus significantly limit the accessible pressure and temperature range. In addition, accurate measurement of pressure at high temperature has been an ongoing problem in resistive heated DACs but is now actively being addressed by the community.[18–22] In contrast to the other two techniques mentioned above, the externally heated DAC experiment offers good temperature and pressure control and can reach much higher pressures then the LVP. Furthermore, the development of sintered nanodiamond anvils could significantly expand the accessible pressure temperature range because the high temperature strength of the anvils can be significantly improved.[23,24] In the future, a combination of experiments on large and well-controlled samples in a resistively heated radial diffraction setup and higher temperature laser-heated measurements will allow the study of plasticity at pressures and temperatures relevant to the Earth's deeper mantle. More generally, the technique could also be useful to

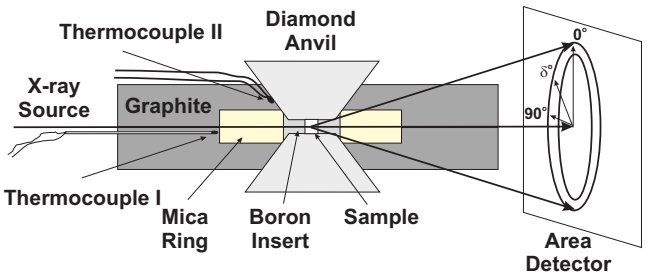

FIG. 1. (Color online) Setup of the RH-RXD-DAC experiment. The polycrystalline sample is confined under nonhydrostatic stress between the two diamond anvils. A monochromatic x-ray beam is sent through the gasket, perpendicular to the compression direction. Microscopic properties of the sample are studied with x-ray diffraction by analyzing the variation in the diffraction spectra as a function of the azimuthal angle δ.

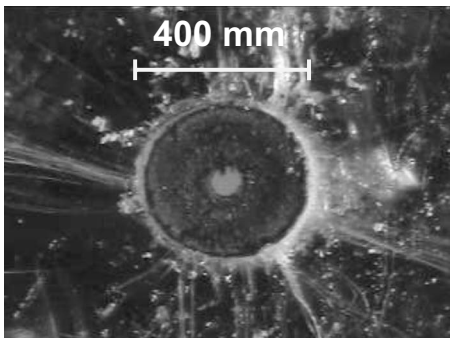

FIG. 3. Gasket assembly consisting of an amorphous boron disk positioned on the diamond anvils and surrounded by a fluorine mica for support of the insert.

study the plasticity of materials relevant to various branches of material sciences, such as superhard materials for which *in situ* characterization of strength and plastic properties are absolutely necessary.[25–27]

In this paper, we present a new radial diffraction technique that allows measurement of textures and stress at simultaneous high pressure and high temperatures in the DAC using an external resistive graphite heater. We demonstrate the current capability of the technique by measuring textures of Fe and its high-pressure polymorphs at simultaneous high pressure and high temperatures.

II. EXPERIMENTAL METHOD

A. Resistive-heated DAC for radial diffraction x-ray experiments

The technique presented here allows us to perform radial x-ray diffraction (RXD) at simultaneous high pressures and high temperatures. It combines three existing techniques: (a) amorphous boron gaskets that allow radial access to the sample,[9] (b) externally graphite heated gaskets,[28] and (c) membrane devices for accurate control of pressure.[29]

In order to accommodate the resistive heating setup and membrane control we designed a new Mao–Bell type DAC [Figs. 2(A) and 2(B)] that will be called resistive-heated-radial-x-ray-diffraction-diamond-anvil-cell (RH-RXD-DAC). In contrast to a conventional Mao–Bell-type cell, the new cell has openings on two sides that allow collection of diffraction patterns perpendicular to the loading axis.

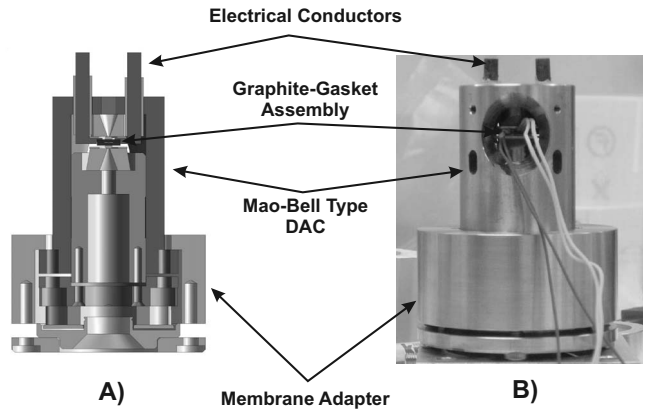

FIG. 2. Three-dimensional (A) cross section and (B) image of the new RH-RXD-DAC for radial diffraction at simultaneous high pressure and high temperature.

Heating of the sample is achieved by using graphite heaters that surround the gasket assembly. The front of the cell has been further modified to accept two molybdenum rods that supply power to the graphite heater. The ends of the molybdenum rods are machined to a perpendicular extension with a step. This holds the graphite heater in place when the piston of the DAC presses against the graphite. The graphite heater consists of two pieces of flexible graphite foil with 1 mm thickness (Alfa Aesar, 97% pure, metal basis) that sandwiches the gasket assembly. The graphite and the gasket assembly are isolated from the tungsten carbide seats by a thin disk of sintered alumina (McDanel Advanced Ceramics Technologies, 99% purity). Prior to sample loading the graphite foil is indented between the diamonds with a thick stainless steel gasket in place of the final gasket assembly. This process shapes the graphite foil, provides a tight contact between the diamonds and the graphite, and allows enough space to position the final gasket assembly.

The gasket consists of a 50 μm thick amorphous boron gasket insert,[9] 400 μm in diameter, with a 50 μm diameter hole that serves as sample chamber (Fig. 3). The kapton sheet that has been used to support the boron insert in RXD experiments at 300 K is replaced by a fluorine bearing mica sheet of 100 μm thickness (H. C. Materials Corporation). The melting temperatures of this fluorine mica (1373 K) is significantly higher than the maximum working temperature of kapton ($\sim$500 K), extending the accessible temperature range in the experiment. Moreover, this material forms a single crystal with a strongly anisotropic crystal structure whose contribution to diffraction is limited because the sheet structure is positioned parallel to the incoming beam, preventing intense basal x-ray diffraction. Finally, a small channel is cut into the graphite heater along the path of the incident beam to avoid significant diffraction from graphite.

In order to prevent the piston and the cylinder from sticking to one another at high temperature and thus preventing the increase and decrease in pressure during the experiment, we use Molykote 1000 Paste (Dow Corning) as a lubricant and heat the outside of the cylinder of the DAC with a strip heater to a maximum of 673 K.

Fine pressure tuning in the cell is provided by adapting the RH-RXD-DAC with a membrane similar to that devel-

oped by the high-pressure group at Lawrence Livermore National Laboratory (LLNL). This allows a remote control of pressure during the experiment.

B. *In situ* x-ray diffraction

We preformed *in situ* x-ray diffraction at beamline 16 BMD of the High-Pressure Collaboration Access Team (HP-CAT), Advanced Photon Source (APS), Argonne National Laboratory (ANL). In the experiment the wavelength of the 15×15 μm^2 monochromatic x-ray beam was tuned to 0.38745 Å at which it offered an optimal flux of $\sim2\times10^8$ photons/sec and resulted in a collection time of 15 min. Data were collected on a 3450×3450 pixel Mar 345 image plate. Sample to detector distance (285.943 mm), detector tilt, and pixel size ratios were calibrated using a CeO_2 standard from NIST (674b).

Sample was a pure commercial powder of iron (Alfa Aesar, 99.9 % purity) with a starting grain size of 1–2 μm. In this run, a small piece of 5 μm thick gold foil was added for additional pressure calibration but could not be seen on the x-ray diffraction images.

C. Temperature in the radial diffraction DAC

The graphite foil was heated through an ultrastable dc power supply from Hewlett Packard with a power range of 0–8 V and 0–220 A (type A6607). Power was increased remotely through an external voltage control provided by the experimental physics and industrial control system (EPICS) at the beamline control area.

Temperature was measured with two Pt–Pt13Rh (type R) thermocouples. The first thermocouple was positioned on the diamond facet of the anvil on the cylinder side of the cell, about half way to the tip. The second thermocouple was located between the two pieces of graphite foil, close to the fluorine bearing mica (Fig. 1). The electro motoric force (EMF) of the thermocouples was measured with a Keithley 7200 equipped with an internal cold junction correction board. The accuracy of the thermocouple reading is +/−5 K.

D. Data processing

Diffraction images were quantitatively analyzed for cell parameters, phase proportions, texture, and lattice strains using the Rietveld method as implemented in the software package MAUD (Ref. 30) according to the procedure described in Ref. 31. Diffraction images were integrated over 5° increments of the azimuth angle, resulting in 72 slices. Data were fit using a bcc, fcc, and hcp structure with adjustable phase ratios. The variations in peak positions with azimuth were adjusted assuming

$$d_m(hkl,\psi) = d_P(hkl)[1 + (1 - \cos^2\psi)Q(hkl)],$$

where ψ represents the angle between the diffracting plane normal and the maximum stress direction, $d_m(hkl,\psi)$ is the measured d-spacing for the (hkl) line diffraction at ψ, $d_p(hkl)$ is the hydrostatic d-spacing of the (hkl) line and is calculated from the hydrostatic lattice parameter, and $Q(hkl)$ is the lattice strain parameter. Values of $Q(hkl)$ can then be used to analyze the stress state of the sample using elastic lattice strain theories[32] or elasto-plastic self-consistent models.[33] CPOs were fitted using the E-WIMW algorithm assuming cylindrical symmetry about the compression direction and using an orientation distribution function (ODF) resolution of 7.5°.

Refinements for the bcc phase were based on measurements on the 110, 200, and 211 diffraction lines. Refinements for the fcc phase were based on measurements on the 111, 200, and 220 diffraction lines. Refinements for the hcp phase were based on measurements on the $10\bar{1}0$, 0002, $10\bar{1}1$, $10\bar{1}2$, and $11\bar{2}0$ diffraction lines.

E. Pressure at high temperatures

Measuring pressure at high temperatures has been a long standing problem for resistive heated experiments. Spectroscopic methods have been used to determine the accurate pressure using fluorescence shifts in ruby, $SrB_4O_7:Sm^{2+}$ or yttrium aluminum garnet crystals.[18–20] More recently shifts in the first order Raman peaks of diamond[34] and cubic boron nitride[20] at high temperature have also been used. Alternatively, one may determine pressure using a *P-V-T* thermal equation of state (EoS) of an internal standard such as Au or Pt. The latter has been established by using multiple pressure calibrants to produce an internally consistent set of high pressure and temperature EoS.[21,22]

In the present experiment, we decided to calibrate pressures using x-ray diffraction of an internal standard. Since gold could not be seen in our diffraction patterns (even at 300 K and 1 bar), we decided to use the EoS of the sample itself, iron, in the bcc structure,[35] and later hcp structure,[36] to estimate pressure at any given temperature during the experiment. To correct for the effect of nonhydrostatic stresses, pressures were calculated using the hydrostatic cell parameters of bcc and hcp iron as derived from the MAUD refinements. Fortunately, in the entire pressure and temperature range covered in this run, either bcc or hcp coexists beyond their stability limit and allowed us to calibrate pressure within the stability field of the fcc phase. The temperature pressure path explored during the experiment can be seen in Fig. 5.

III. RESULTS AND DISCUSSION

A. Accuracy of temperature measurements in the RH-RXD-DAC

Because of the high thermal conductivity of diamonds and complexity of the sample assembly, temperature measurements with thermocouples that do not directly surround the sample have been questioned in the past.[37] To investigate this issue, we measured the melting temperature of Pb (605 K), Al (933.2 K), and NaCl (1077 K) in a second membrane controlled graphite resistively heated DAC that was used recently.[28] This membrane cell uses the exact same heating assembly and similar thermocouple positions as those described in this work. Thus, it represents an accurate test of our capability to measure temperatures in the low to medium temperature range.

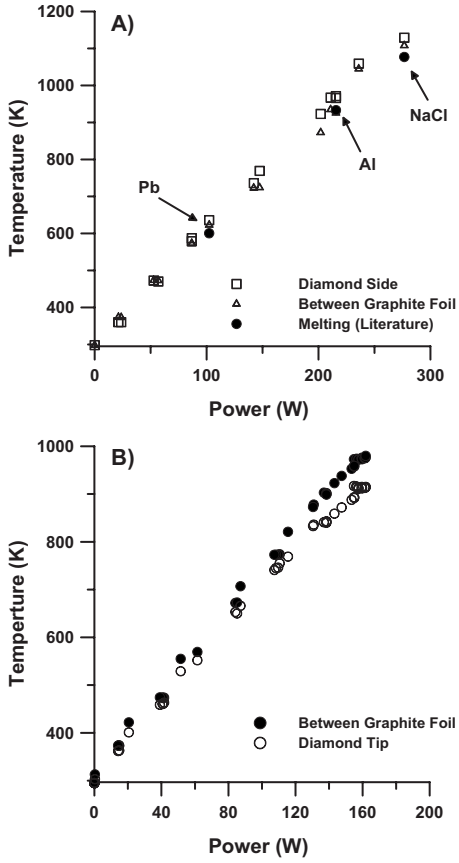

FIG. 4. (A) Ambient pressure temperature measurements as a function of power in the resistive heated DAC. Onset of melting was observed optically through a microscope and is indicated by arrows in the figure. Differences between the melting temperatures reported in the literature and those measured using the thermocouple positioned between the graphite foil for Pb, Al, and NaCl are −22, 2, and −30 K, respectively. (B) High-pressure temperature measurements as a function of power in the radial diffraction membrane driven Mao–Bell type DAC. The maximum difference between the temperatures recorded by both thermocouples (see text) is 66 K recorded at the highest temperature.

Melting was observed optically through a Navitar zoom microscope with a maximum primary magnification of 20×. Samples of Al and Pb were separated in the sample chamber by NaCl to avoid reaction between the different standards during heating. Even though we did not determine the pressure in the sample chamber after closing the DAC, we observed small holes indicating that the sample was not compressed and did not show any considerable pressure. The sample chamber was illuminated by reflected and transmitted light. Onset of melting was determined by observing the appearance of movements in the liquid phase and changes in the sample surface texture. Both approaches are commonly used to determine melting of metals in laser heated DAC experiments with accuracy in the ten's of Kelvin.[38]

Temperatures recorded on both thermocouples at zero pressure are plotted as a function of power in Fig. 4(A). Up to 1077 K the discrepancy between the temperature recorded at the onset of melting and the melting temperature reported in the literature are within +2 to −30 K for the thermocouple positioned between the two pieces of graphite foil and up to 60 K for the thermocouple positioned on the facet of the diamond.

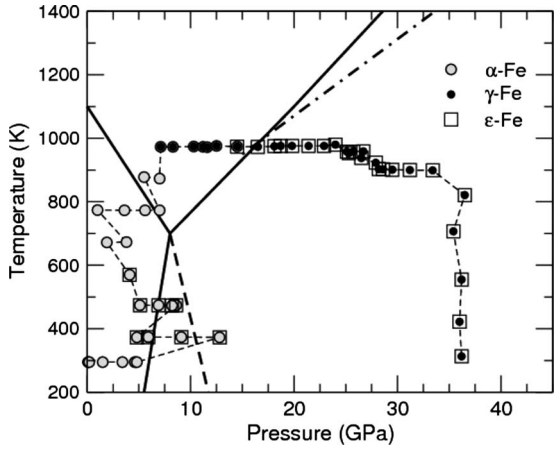

FIG. 5. Pressure-temperature path explored during the second radial diffraction experiment. Grey circles denote the presence of bcc iron (α-Fe), open squares for hcp iron (ε-Fe), and black circles for fcc iron (γ-Fe). fcc iron coexists with hcp iron past its stability limit until the end of the experiment. Phases in the sample were identified from the diffraction images. Solid and dotted lines are the iron phase diagram upon compression and decompression, respectively, as published in Ref. 36. Dashed-dotted line represents the hcp-fcc phase boundary (Ref. 35).

These measurements imply that temperatures recorded by the thermocouple positioned between the two graphite foils are within 30 K of the real temperature. Note that the difference between melting temperatures reported in the literature and those measured by the second thermocouple, positioned about 1 mm away from the diamond tip, only extends to +60 K. This relatively small difference indicates that the gasket assembly and the top part of the diamond are very efficiently heated by the graphite foil and that temperature gradients in the gasket, sample, and diamond tip area are relatively small.

Temperatures measured in both thermocouples during the RH-RXD-DAC experiment on iron are plotted as a function of power in Fig. 4(B). In contrast to the melting experiment above, temperatures recorded by the thermocouple positioned between the two graphite foils are always higher than those recorded at the facet of the diamond. This difference can be explained by the fact that the thermocouple at the facet of the diamond is not always positioned precisely the same way. In addition we find that the shape of the tungsten carbide seat, i.e., the opening of the seat, significantly affects the amount of heat being carried away from the back of the diamond anvil. The opening of the seat in the DAC used for the melting experiment is much smaller than that of the radial diffraction RH-RXD-DAC seats. Hence, the temperatures recorded at the facet of the diamond anvil of the radial diffraction cell are lower. Nevertheless, the difference in temperatures recorded by the two thermocouples never exceeds 62 K. This indicates fairly homogeneous heating during the experiment.

B. Phase diagram and equation of state of fcc iron

Table I lists the refined cell parameters obtained from positions of the diffraction peaks of bcc, fcc, and hcp iron as a function of pressure and temperature during the experiment. We obtain small errors for the cell parameters of bcc

TABLE I. Cell parameters refined from peak positions of bcc, fcc, and hcp iron. Temperature was measured with a thermocouple. Pressure was calculated using the cell parameters of bcc and hcp iron and their respective high-pressure and high-temperature EoS (Refs. 35 and 36). The error in the temperature measurement is estimated to be +/−30 K and the error in the pressure calculation is +/−0.7 GPa based on an average error of 0.004 Å in the cell parameters. Errors for the cell parameters obtained for bcc Fe before the appearance of other phases are approximately 0.001 Å. When multiphase aggregate is present, errors on cell parameters are on the order of 0.004 Å.

					Fe (hcp)	
Image	*T* (K)	*P* (GPa)	Fe (bcc) *a* (Å)	Fe (fcc) *a* (Å)	*a* (Å)	*c* (Å)
3	295	0.1	2.866			
13	295	0.2	2.865			
22	295	1.5	2.858			
24	295	3.4	2.848			
28	295	4.6	2.842			
31	295	4.8	2.841			
35	373	12.8	2.807		2.438	4.028
36	374	9.1	2.823		2.454	3.978
37	374	5.9	2.838		2.468	3.992
38	373	4.8	2.843		2.473	4.096
40	474	8.6	2.828		2.464	4.118
41	473	8.2	2.830		2.468	4.117
42	474	6.9	2.836		2.473	4.136
43	474	5.1	2.845		2.477	4.151
45	570	4.1	2.853		2.497	4.180
46	672	1.9	2.869			
47	673	3.8	2.858			
48	774	1.0	2.878			
49	773	3.6	2.863			
50	773	5.6	2.852			
51	773	7.0	2.845			
53	878	5.5	2.856			
54	873	7.0	2.848			
56	973	7.1	2.851	3.619		
57	973	8.3	2.845	3.606		
58	974	10.3	2.835	3.580		
59	973	11.2	2.831	3.566		
60	972	11.6	2.829	3.558		
62	976	12.5	2.825	3.546		
63	974	14.5	2.818	3.529	2.481	4.030
64	973	16.4		3.519	2.476	4.012
65	975	18.0		3.508	2.472	3.993
66	976	18.5		3.504	2.470	3.990
67	976	19.9		3.498	2.465	3.981
68	976	21.3		3.491	2.460	3.970
69	976	22.9		3.484	2.455	3.959
70	980	24.0		3.476	2.451	3.953
71	953	25.2		3.472	2.446	3.944
72	958	25.0		3.470	2.447	3.946
73	958	25.6		3.470	2.445	3.942
74	959	26.6		3.465	2.442	3.936
75	938	26.4		3.465	2.442	3.936
76	923	27.8		3.465	2.438	3.924
77	903	28.2		3.459	2.436	3.922
78	902	28.4		3.455	2.435	3.921
79	901	29.4		3.453	2.432	3.916
80	900	31.0		3.444	2.427	3.908
81	899	33.2		3.434	2.421	3.897
83	821	36.6		3.419	2.410	3.876
85	707	35.4		3.419	2.410	3.877
87	555	36.1		3.413	2.406	3.865
88	422	36.0		3.409	2.404	3.860

TABLE I. (*Continued.*)

Image	*T* (K)	*P* (GPa)	Fe (bcc) *a* (Å)	Fe (fcc) *a* (Å)	Fe (hcp) *a* (Å)	Fe (hcp) *c* (Å)
89	313	36.2		3.410	2.402	3.855

iron before the appearance of other iron phases but rather large errors later on. This is due to inconsistencies between the cell parameters obtained from various diffraction lines, which could be due to the presence of a mixed phase.

In our experiment, the transition from the bcc to the fcc phase of iron occurred at temperatures higher than those reported in the literature[36,39,40] (Fig. 5). However, phase transitions in iron are known to be very sensitive to both kinetics[36] and stress.[41] Our experiment was designed to prove the capabilities of the instrument. As such, we did not perform multiple transition cycles and long heating periods necessary for full phase conversions and proper phase diagram analysis. Therefore, small discrepancies between our experiments and reported phase boundaries can be attributed to kinetics and stress.

Our cell parameters for fcc iron are also significantly different from those reported in the literature.[40,41] This is particularly true at low pressures. Differences between our measured cell parameters and the published EoS (Ref. 40) decrease with increasing pressure. It is known that coexistence of two or three phases associated with a phase transition can cause volume anomalies due to the difference in linear compressibility and thermal expansivity. This can explain the observed discrepancy. Proper measurement of the EoS of fcc Fe should be performed with better phase conversion, longer heating periods, and minimal stress conditions.

C. Diffraction and texture development in iron at high pressure and temperature

The greatest challenge collecting and processing radial diffraction data from a DAC originates from the background created by material that lies in the diffraction path. In the case of the RH-RXD-DAC, graphite, fluorine mica, and amorphous boron contribute to the background (Fig. 1).

Figure 6 shows the diffraction image collected at 976 K and 12.5 GPa. The diffraction image clearly shows powder diffraction peaks corresponding to the 111, 200, and 220 lines of fcc iron and 110, 200, and 211 lines of bcc iron. Diffraction from graphite is limited to the most intense 002 peak. Single crystal spots of mica are significant but localized; they can be easily filtered out during the processing. Due to grain growth and recrystallization, iron diffraction lines are spotty. Nevertheless, variations in diffraction intensities with orientation can be observed. They are related to CPO in the polycrystalline sample. Similarly, slight variations in peak positions with orientations can be used to model the differential stress supported by the sample.

Reliable textures can be extracted. Figure 7, for instance, presents inverse pole figures of the compression direction obtained for bcc and fcc iron at 12.5 GPa and 976 K and fcc and hcp iron at 33.2 GPa and 899 K. ODFs were obtained directly in MAUD and further smoothed with a 10° gauss filter in BEARTEX.[42]

Upon compression, bcc iron develops a mixed {100} and {111} texture that is compatible with previous observations on bcc iron[16,43] and interpreted as slip along {110}⟨111⟩. When bcc iron is heated between 295 and 976 K, we observe a recrystallization of the sample, as evident by the spotty pattern in Fig. 6. The {100} and {111} maxima are preserved during heating.

Texture obtained after formation of fcc iron shows a maximum near {110} with minima near {100} and {111}. This texture is typical for fcc metals in compression with slip on {111}⟨110⟩,[16] but could also be related to texture being transmitted from the bcc to the fcc phase according to the Kurdjumow–Sachs orientation relations.[44]

Textures obtained in hcp iron seem different from those reported before.[5,16,34] Further study and modeling will be re-

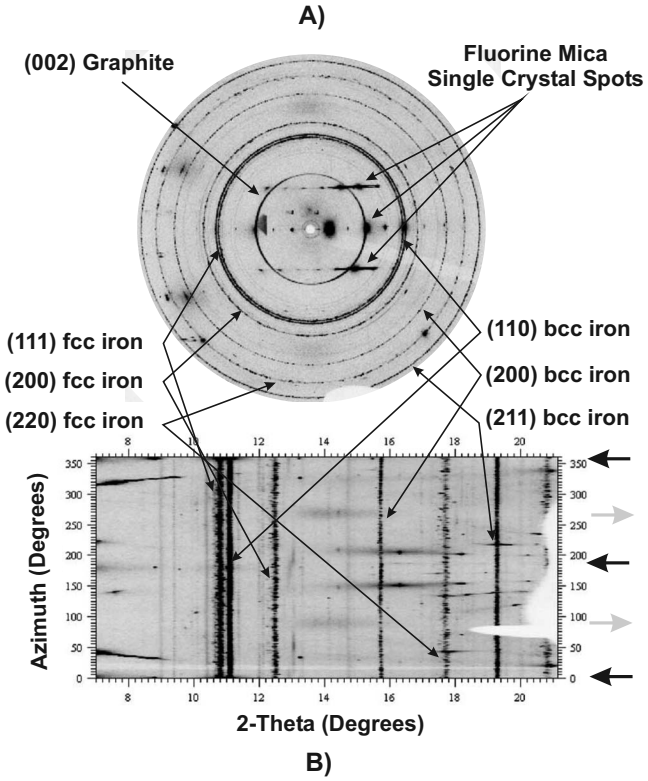

FIG. 6. (A) Radial diffraction image and (B) unrolled diffraction image of fcc iron at 12.5 GPa and 976 K and in the graphite resistive heated Mao–Bell type DAC. Besides diffraction peaks of fcc (111, 200, and 220) and bcc Fe (110, 200, and 211), one can see powder diffraction peaks of graphite (002) and single crystal diffraction spots of fluorine bearing mica.

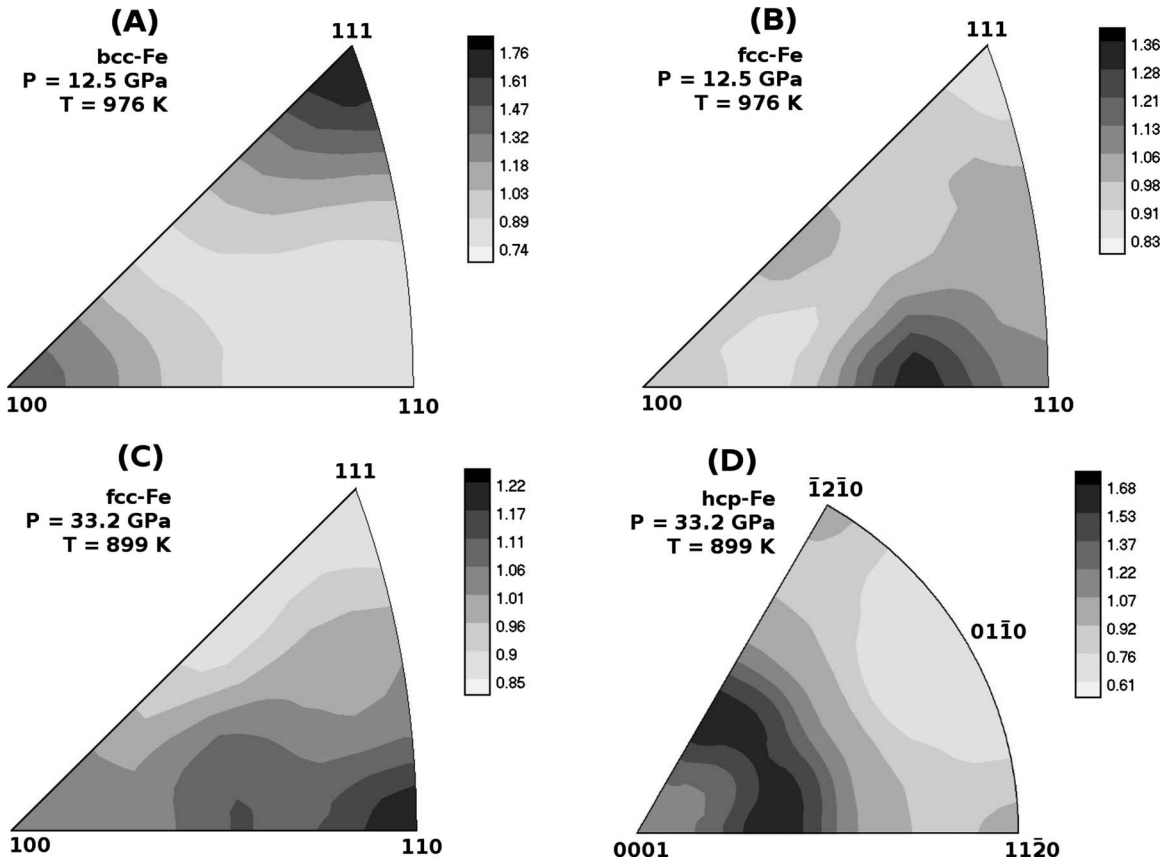

FIG. 7. Inverse pole figure of the compression direction for [(A) and (B)] bcc and fcc iron at 12.5 GPa and 976 K and [(C) and (D)] fcc and hcp iron at 33.2 GPa and 899 K. Equal area projection. Linear polar density scale in multiples random distribution.

quired for full interpretation, which goes beyond the scope of this paper.

D. Application of the instrumentation

One of the primary applications of radial diffraction DAC experiments is the investigation of deformation mechanisms and possible preferred orientation patterns of rocks in the deep Earth, e.g., the lower mantle and the core. Today, radial diffraction is the only direct method to probe plastic processes at pressures of the Earth's lower mantle. Until now, an obvious limitation in using ambient temperature results of CPO formed in the DAC was the lack of temperature. It was therefore desirable to develop reliable heating methods for radial diffraction. The technique presented here will allow the investigation of deformation of minerals up to temperatures of about 1500 K, a temperature at which diffusion processes that are critical for plasticity can become active.

The instrumentation presented here can also be used to study the strength of newly designed superhard materials.[25–27] Most of these studies are limited to measurements of quasihydrostatic EoSs for extraction of isothermal bulk moduli. This is insufficient to assess the strength and behavior of the material under complex conditions. Using the new instrumentation, one could study the strength and microscopic plastic deformation mechanisms under various conditions of pressure and temperature. This will provide valuable information for understanding the plastic behavior of industrially relevant materials.

IV. CONCLUSION

We designed a DAC experimental setup that allows the collection of x-ray diffraction data in a radial geometry from samples plastically deformed at simultaneous high pressure and high temperature. The setup was successfully tested up to temperatures of 1100 K and pressures of 36 GPa.

Errors in temperature measurements are within +/−30 K in the entire temperature range explored. Moreover, temperatures measured at ~1 mm away from the tip of the diamond on the diamond facet show a temperature difference of only +/−60 K, indicating that the gasket and tips of the diamonds are heated very homogeneously.

The instrumentation allows the collection of radial x-ray diffraction data of sufficient quality for the extraction of texture and stress information using the Rietveld refinement program "MAUD." Detailed analysis of the data presented here will be discussed elsewhere. However, preliminary analysis indicates the presence of a strong {110} texture in fcc iron, compressed in the DAC between 7.1 and 12.5 GPa at 970 K, after the transformation from bcc iron.

This new instrumentation can now be used for the study of plastic properties of minerals and other materials at simultaneous high-pressure and high-temperature conditions.

ACKNOWLEDGMENTS

The authors like to thank W. Yang and E. Rod for their technical support at the beamline and during the experiment. We also thank L. Dubrovinsky for helpful suggestions regarding the resistive heated DAC and the anonymous reviewer for critical comments that improved the quality of the manuscript. This work was performed at HPCAT (Sector 16), Advanced Photon Source (APS), Argonne National Laboratory. HPCAT is supported by DOE-BES, DOE-NNSA, NSF, and the W.M. Keck Foundation. APS is supported by DOE-BES under Contract No. DE-AC02-06CH11357. W.J.E. and H.C. gratefully acknowledge the support from DOE/NNSA Science Campaign-2 (Program Manager—Dr. Kimberly Budil). Their contribution was performed under the auspices of the U.S. DOE by LLNL under Contract No. DE-AC52-07NA27344. L.M. and H.-R.W. acknowledge the support from CDAC and NSF (Grant No. EAR-0836402). S.M. acknowledges support from the ANR program DiUP.

[1] R. J. Hemley and H. K. Mao, Miner. Mag. **66**, 791 (2002).
[2] G. L. Kinsland and W. A. Bassett, J. Appl. Phys. **48**, 978 (1977).
[3] R. J. Hemley, H. K. Mao, G. Shen, J. Badro, P. Gillet, M. Hanfland, and D.Häusermann, Science **276**, 1242 (1997).
[4] H. K. Mao, J. Shu, G. Shen, R. J. Hemley, B. Li, and A. K. Singh, Nature (London) **399**, 280 (1999).
[5] H. R. Wenk, S. Matthies, R. J. Hemley, H. K. Mao, and J. Shu, Nature (London) **405**, 1044 (2000).
[6] S. Merkel, H. R. Wenk, J. Shu, G. Shen, P. Gillet, H. K. Mao, and R. J. Hemley, J. Geophys. Res. **107**, 2271 (2002).
[7] H. K. Mao, J. Shu, Y. Fei, J. Hu, and R. J. Hemley, Phys. Earth Planet. Inter. **96**, 135 (1996).
[8] J. F. Lin, J. Shu, H. K. Mao, R. J. Hemley, and G. Shen, Rev. Sci. Instrum. **74**, 4732 (2003).
[9] S. Merkel and T. Yagi, Rev. Sci. Instrum. **76**, 046109 (2005).
[10] H. R. Wenk, I. Lonardelli, S. Merkel, L. Miyagi, J. Pehl, S. Speziale, and C. E. Tommaseo, J. Phys.: Condens. Matter **18**, S933 (2006).
[11] S. Merkel, A. K. McNamara, A. Kubo, S. Speziale, L. Miyagi, Y. Meng, T. S. Duffy, and H.-R. Wenk, Science **316**, 1729 (2007).
[12] S. Merkel, A. Kubo, L. Miyagi, S. Speziale, T. S. Duffy, H.-K. Mao, and H.-R. Wenk, Science **311**, 644 (2006).
[13] D. Yamazaki and S. Karato, Rev. Sci. Instrum. **72**, 4207 (2001).
[14] Y. Wang, W. B. Durham, I. C. Getting, and D. J. Weidner, Rev. Sci. Instrum. **74**, 3002 (2003).
[15] M. Kunz, W. A. Caldwell, L. Miyagi, and H.-R. Wenk, Rev. Sci. Instrum. **78**, 063907 (2007).
[16] L. Miyagi, M. Kunz, J. Knight, J. Nasiatka, M. Voltolini, and H. R. Wenk, J. Appl. Phys. **104**, 103510 (2008).
[17] S. Petitgirard, I. Daniel, Y. Dabin, H. Cardon, R. Tucoulou, and J. Susini, Rev. Sci. Instrum. **80**, 033906 (2009).
[18] F. Datchi, R. LeToullec, and P. Loubeyre, J. Appl. Phys. **81**, 3333 (1997).
[19] C. Sanchez-Valle, I. Daniel, B. Reynard, R. Abraham, and C. Goutaudier, J. Appl. Phys. **92**, 4349 (2002).
[20] A. F. Goncharov, J. C. Crowhurst, J. K. Dewhurst, S. Sharma, C. Sanloup, E. Gregoryanz, N. Guignot, and M. Mezouar, Phys. Rev. B **75**, 224114 (2007).
[21] Y. Fei, A. Ricolleau, M. Frank, K. Mibe, G. Shen, and V. Prakapenka, Proc. Natl. Acad. Sci. U.S.A. **104**, 9182 (2007).
[22] C.-S. Zha, K. Mibe, W. A. Bassett, O. Tschauner, H.-K. Mao, and R. J. Hemley, J. Appl. Phys. **103**, 054908 (2008).
[23] T. Irifune, A. Kurio, S. Sakamoto, T. Inoue, H. Sumiya, and K. Funakoshi, Phys. Earth Planet. Inter. **143–144**, 593 (2004).
[24] Y. Nakamoto, H. Sumiya, T. Matsuoka, K. Shimizu, T. Irifune, and Y. Ohishi, Jpn. J. Appl. Phys., Part 2 **46**, L640 (2007).
[25] C. T. Liu and J. O. Stiegler, Science **226**, 636 (1984).
[26] H. Y. Chung, M. B. Weinberger, J. B. Levine, A. Kavner, J. Yang, S. H. Tolbert, and R. B. Kaner, Science **316**, 436 (2007).
[27] V. Solozhenko, O. O. Kurakevych, D. Andrault, Y. Le Godec, and M. Mezouar, Phys. Rev. Lett. **102**, 015506 (2009).
[28] G. Shen, H. P. Liermann, S. Sinogeikin, W. Yang, X. Hong, C.-S. Yoo, and H. Cynn, Proc. Natl. Acad. Sci. U.S.A. **104**, 14576 (2007).
[29] R. Letoullec, J. P. Pinceaux, and P. Loubeyre, High Press. Res. **1**, 77 (1988).
[30] L. Lutterotti, S. Matthies, H.-R. Wenk, A. S. Schultz, and J. W. Richardson, J. Appl. Phys. **81**, 594 (1997).
[31] L. Miyagi, S. Merkel, T. Yagi, N. Sata, Y. Ohishi, and H.-R. Wenk, J. Phys.: Condens. Matter **18**, S995 (2006).
[32] A. K. Singh, C. Balasingh, H. K. Mao, R. J. Hemley, and J. Shu, J. Appl. Phys. **83**, 7567 (1998).
[33] S. Merkel, C. N. Tomé, and H. R. Wenk, Phys. Rev. B **79**, 064110 (2009).
[34] F. Occelli, P. Loubeyre, and R. LeToullec, Nature Mater. **2**, 151 (2003).
[35] T. Komabayashi and Y. Fei, "Internally consistent thermodynamic database for iron to the Earth's core conditions," J. Geophys. Res., [Solid Earth] (submitted).
[36] T. Uchida, Y. Wang, M. Rivers, and S. R. Sutton, J. Geophys. Res. **106**, 21799 (2001).
[37] N. Dubrovinskaia and L. Dubrovinsky, Rev. Sci. Instrum. **74**, 3433 (2003).
[38] D. Errandonea, B. Schwager, R. Ditz, C. Gessmann, R. Boehler, and M. Ross, Phys. Rev. B **63**, 132104 (2001).
[39] R. Boehler, Geophys. Res. Lett. **13**, 1153 (1986).
[40] T. Komabayashi, Y. Fei, Y. Meng, and V. Prakapenka, Earth Planet. Sci. Lett. **282**, 252 (2009).
[41] R. Boehler, N. Von Bargen, and A. Chopelas, J. Geophys. Res. **95**, 21731 (1990).
[42] H. R. Wenk, S. Matthies, J. Donovan, and D. Chateigner, J. Appl. Crystallogr. **31**, 262 (1998).
[43] S. Merkel, H.-R. Wenk, P. Gillet, H. K. Mao, and R. J. Hemley, Phys. Earth Planet. Inter. **145**, 239 (2004).
[44] G. Kurdjumow and G. Sachs, Z. Phys. **64**, 325 (1930).